2022 IEEE International Conference on
Systems, Man, and Cybernetics (SMC)

Multi-Domain Simulation of Human Mechanics for Dynamic Analysis

Tobias Treichl
Institute of System Dynamics and Control
German Aerospace Center
Wessling, Germany
ORCID: 0000-0001-7111-8805

Daniel Milz
Institute of System Dynamics and Control
German Aerospace Center
Wessling, Germany
ORCID: 0000-0001-9704-2036

Tobias Bellmann
Institute of System Dynamics and Control
German Aerospace Center
Wessling, Germany
ORCID: 0000-0002-5897-6191

Andreas Seefried
Institute of System Dynamics and Control
German Aerospace Center
Wessling, Germany
ORCID: 0000-0002-8367-2704

2022 IEEE International Conference on Systems, Man, and Cybernetics (SMC) | 978-1-6654-5258-8/22/$31.00 ©2022 IEEE | DOI: 10.1109/SMC53654.2022.9945492

***Abstract*—Digital human models (DHM) offer a great possibility of design evaluation for products humans interact with. One field to apply DMH's is the dynamic analysis of human-machine interaction. Thereby, the dynamics of the human body can significantly influence the entire system behavior and thus it is important to consider during the design process. For the modeling language Modelica no simulation library for this application is available, so far. The language is especially suitable for the simulation across different domains, which makes a DHM in Modelica useful. In this paper a DHM predicting the dynamic behavior of the human body during human-machine interaction is implemented in Modelica. It consists of a multi-body skeleton model, an inverse kinematics algorithm for the limbs and a controller for the skeleton joints inspired by human motor control. The capability of the proposed simulation approach to take the relevant dynamical properties of the human body and motor control into account is demonstrated in a use-case simulation. As use-case the aircraft-pilot coupling during a strong gust acting on a sports aircraft is investigated.**

***Index Terms*—digital human model, dynamic analysis, pilot-aircraft coupling, modelica**

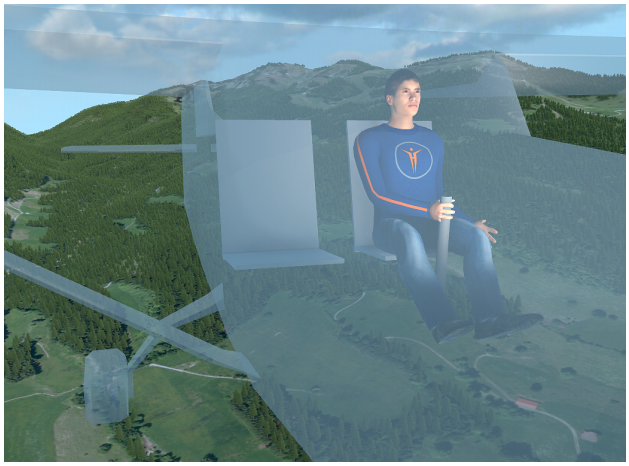

Fig. 1. Visualization of the presented DHM in the use-case scenario with the DLR Visualization 2 Library [19]. As use-case the aircraft-pilot interaction during a gust is investigated.

I. Introduction

Digital human models (DHM) have become an important part of research and development in engineering, which can be seen by the amount of software for DHM's available on the market. Siemens PLM [6], AnyBody [5] , Ramsis [4] or OpenSim [7] are examples of software used for the simulation of the human body in areas like comfort evaluation, production planning and medicine. Another field to apply DHM's lies in the dynamic analysis of human-machine systems with the focus on the dynamic interaction of humans with their environment. Every system representing a dynamic environment to the human body is a potential area of application for such DHM's. Examples reach from the safety analysis of fun rides over the assessment of vehicle control tasks executed by the human to the simulation of aircraft-pilot-interaction. The human body mechanics can thereby significantly influence the whole human machine interconnection. This interaction, can be shown e.g. for air vehicles, is in the worst case leading to unstable behavior of the closed loop between pilot and aircraft, known as aircraft-pilot coupling [30]. Thus, if a human feedback loop exists around any system, the impact of the human body dynamics on the closed loop system behavior is important to be considered.

It is relevant to be able to address these effects in dynamic analysis to identify possible unstable operating regions. It can also be useful to identify situations in dynamic analysis where the needed forces to execute intended movements exceed the human's capabilities.

In literature there are different approaches to simulate the human behavior in dynamic human-machine interaction. One is to model the human as a blackbox, using transfer functions [8], [20], [9]. This approach offers the advantage of low computational cost, but is only capable to a limited degree to cover the biomechanics of the pilot. Another approach are multi-body models. Models using this approach differ in the simplification of the skeleton and the modeling of muscles. The most detailed models nowadays are musculoskeletal models as found in [30] or [16] where muscles are modeled as one dimensional force elements. Musculoskeletal

models are capable of determining single muscle forces but this comes to the expense of high computational cost and complex control schemes. Less detailed DHMs, where the different muscle groups are represented indirectly through the joint torques, offer the advantage of lower computational cost with no need of a detailed understanding of the underlying muscle activities [11].

In this paper, a DHM implemented in the modeling language `Modelica` is presented. `Modelica` is especially suitable for the simulation across different domains, which makes the DHM versatile. The DHM can therefore easily be coupled with other physical models such as an airplane aerodynamics model or a vehicle dynamics model. The scope of the DHM lies in the simulation of sitting humans during interaction with their environment via the limbs and not on standing or walking processes. Currently no similar models for `Modelica` are available. The here presented DHM can be assigned to the last type of models mentioned above, where muscles are modeled indirectly. The model consists of a simplified, fully parametric skeleton multi-body model, an inverse kinematics (IK) algorithm as well as a proposed controller for the upper and lower limbs inspired by human motor control. The capability of this simulation approach to describe the dynamic interaction of the human body in an aircraft-pilot coupling situation is demonstrated in a use-case simulation. Fig. 1 shows the visualized use-case scenario in which the dynamic behavior of the pilot during a gust on the aircraft is investigated.

II. HumanBody Library for Modelica

This section details the modeling approach of the presented DHM. It starts with the description of the multi-body skeleton model in paragraph II-A. After that in paragraph II-B the IK-algorithm, calculating the reference joint angles of the limbs, is explained. Paragraph II-C describes the human-like control scheme used to control each limbs joints to follow the joint angles calculated by the IK-algorithm.

Position vectors $\boldsymbol{r} \in \mathbb{R}^3$ and orientations matrices $\boldsymbol{T} \in \mathbb{R}^{3\times3}$ in the following are noted in the world coordinate system $\mathcal{F}_W$ unless stated otherwise.

A. Multi-Body Skeleton Model

The skeleton model of the DHM is a simplified multi-body model of the human skeleton. Fig. 2 shows the components comprising the skeleton model. The human skeleton is simplified to 14 joints, illustrated by circles, with a total number of 33 degrees of freedom (DOF). Joints with more than one DOF are modeled as a combination of swivel joints. The simplification of the human skeleton is inspired by the skeleton model in [27] which covers all important joints of the human body. But in contrast to [27] the movement of the shoulders is neglected in this model to keep the number of joint angles to be parameterized manually low.

The segments between the joints are treated as rigid bodies with masses m and inertia Tensors $\boldsymbol{I}$. The origins of the rigid bodies are marked with the gray diamonds. The distribution of the body weight among the rigid bodies matches the weight distribution of an average human [2]. Different weight distributions can be defined if desired.

The lengths of the segments between the joints are parametric. There are six predefined parameter sets for the proportions of the skeleton model. The parameter sets, three each for women and men with the 5^{th}, 50^{th} and 95^{th} percentile of body height, are based on the DIN 33402-2 norm [3].

Fig. 2 also shows that the upper and lower limbs are modeled kinematically equal with seven DOF each. The joints of the limbs are actuated to reach a given time-varying position $\boldsymbol{r}^i_{ref}$ and orientation $\boldsymbol{T}^i_{ref}$ for each hand and foot. The combination of position and orientation is further called a pose. The superscript $i \in [1,2,3,4]$ denotes the limb for which the pose is defined. The reference joint angles $\boldsymbol{q}^i_{ref} \in \mathbb{R}^7$ to define all seven DOF of a limb and to reach the pose given, are calculated by the IK-algorithm from section II-B. The joints of the limbs can be either

- controlled by the controller in section II-C, actuating the joints in a way, that the desired joint angles $\boldsymbol{q}^i_{ref}$ are reached dynamically against potential interference.
- set to the calculated time-varying joint angles $\boldsymbol{q}^i_{ref}$ from the IK in section II-B to result in a desired pose. This can e.g. be used to create a purely kinematic simulation for visualization purposes.
- defined directly as fixed joint angles, if no use of the IK for the concerning limb is required during simulation.

Only the first way is suitable to simulate a dynamic interaction. With the joint torques, coming from the controller, the underlying muscle groups generating these torques are modeled indirectly.

The two joints concerning the torso are parameterized manually by user defined joint angles $\boldsymbol{q}_{torso} \in \mathbb{R}^5$. The skeleton model has up to five physical connections to its environment. One at each hand and foot as well as one at the buttocks (see Fig. 2). The connection at the buttocks is mandatory whereas the other connections are optional. Through cut torques $\boldsymbol{m}^i \in \mathbb{R}^3$ and forces $\boldsymbol{f}^i \in \mathbb{R}^3$, acting on these connections, interaction with the environment is

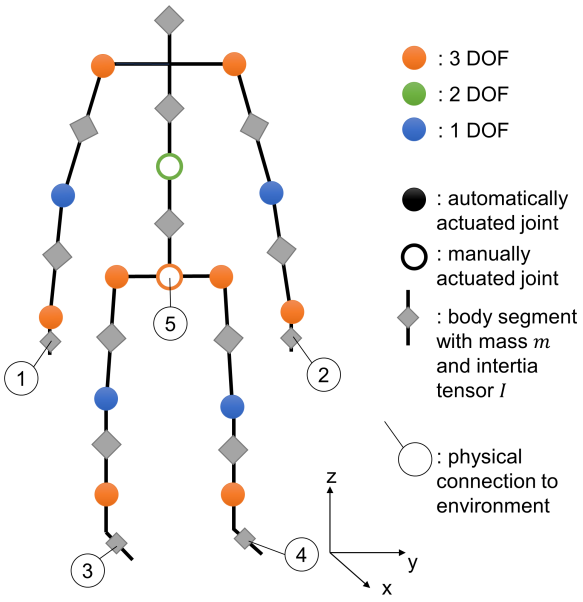

Fig. 2. Simplified multi-body skeleton model of the DHM. It consists of twelve joints at the limbs, controlled automatically via the controller from section II-C, and two manually parameterized joints at the torso. Rigid bodies with a representative mass distribution connect the joints.

possible. At the hands the connections can be e.g. to controls like a flight stick as shown in the use-case from section III. At the buttocks the connection is usually to the seat.

B. Inverse Kinematics (IK) Algorithm

To control each limb the controller requires the reference angles $\boldsymbol{q}^i_{ref}$. They are calculated by the IK algorithm. The position $\boldsymbol{r}^i_{ref}$ and orientation $\boldsymbol{T}^i_{ref}$ define the six DOF of each limb's hand or foot, further called end-effector. For the seven joint angles of each limb there is in general an infinite number of solutions to reach $\boldsymbol{r}^i_{ref}$ and $\boldsymbol{T}^i_{ref}$ if they are in range of the limb.

The IK algorithm calculates $\boldsymbol{q}^i_{ref}$ for each limb in a way that the superfluous DOF is used to obtain a realistic limb posture with consideration of the joint limits. It is an iterative algorithm based on the damped least squares IK algorithm in [10] and [25]. The least squares problem, solved in each iteration step k, to obtain unique joint angles under the constraint of complying with the joint limits $\boldsymbol{q}^i_{min} \in \mathbb{R}^7$ and $\boldsymbol{q}^i_{max} \in \mathbb{R}^7$ is

$$min\ \frac{1}{2}||\boldsymbol{R} \cdot \Delta\boldsymbol{q}^k_t - \boldsymbol{s}||^2 \tag{1}$$

under the constraints:

$$\boldsymbol{q}^i_{min}[j] \leq \boldsymbol{q}^i_{ref}[j](t - \Delta t) + \Delta\boldsymbol{q}^k_t[j] \tag{2a}$$

$$\boldsymbol{q}^i_{max}[j] \geq \boldsymbol{q}^i_{ref}[j](t - \Delta t) + \Delta\boldsymbol{q}^k_t[j] \tag{2b}$$

with

$$\boldsymbol{R} = \begin{pmatrix} \boldsymbol{J}_{pos} \cdot w_1 \\ \boldsymbol{J}_{or} \cdot w_2 \\ \boldsymbol{I} \cdot \lambda \\ \boldsymbol{P} \cdot w_3 \end{pmatrix} \tag{3a}$$

$$s = \begin{pmatrix} (\boldsymbol{e}_{pos} + \boldsymbol{J}_{pos} \cdot \Delta\boldsymbol{q}^{k-1}_t) \cdot w_1 \\ (\boldsymbol{e}_{or} + \boldsymbol{J}_{or} \cdot \Delta\boldsymbol{q}^{k-1}_t) \cdot w_2 \\ \lambda \cdot \Delta\boldsymbol{q}^{k-1}_t \\ \boldsymbol{P} \cdot \boldsymbol{q}_{guess} \cdot w_3 \end{pmatrix}. \tag{3b}$$

t is the simulation time and Δt is the length of one time step. The notation $[j]$ denotes the j^{th} element of a vector. The iteration starts with the joint angles $\boldsymbol{q}^i_{ref}(t - \Delta t)$ of the last time step. In the iteration process the necessary change of the joint angles $\Delta\boldsymbol{q}^k_t$ is calculated iteratively by solving (1) until $\boldsymbol{r}^i_{ref}$ and $\boldsymbol{T}^i_{ref}$ are reached within a specified error range. Equations (3) show the calculation of the matrix $\boldsymbol{R}$ and the vector $\boldsymbol{s}$. The first two rows of $\boldsymbol{R}$ and $\boldsymbol{s}$ specify the optimization criteria of reaching the position and orientation. $\boldsymbol{e}_{pos} \in \mathbb{R}^3$ and $\boldsymbol{e}_{or} \in \mathbb{R}^4$ are the position and orientation error with

$$\boldsymbol{e}_{pos} = \boldsymbol{r}^i_{ref} - \boldsymbol{r}^i \tag{4}$$

$$\boldsymbol{e}_{or} = \boldsymbol{Q}(\boldsymbol{T}^i_{ref}) - \boldsymbol{Q}(\boldsymbol{T}^i). \tag{5}$$

$\boldsymbol{Q}(\boldsymbol{T})$ are the corresponding quaternions to $\boldsymbol{T}^i_{ref}$ and $\boldsymbol{T}^i$. $\boldsymbol{J}_{pos} \in \mathbb{R}^{3\times7}$ and $\boldsymbol{J}_{or} \in \mathbb{R}^{4\times7}$ are the jacobians of the position and orientation. Information how these quantities are derived can be found in [10]. With w_1 and w_2 the weightings of the two criteria can be adjusted. The third row of $\boldsymbol{R}$ and $\boldsymbol{s}$ forms a damping term with the damping coefficient λ to prevent oscillations near singular configurations like a fully stretched arm. Here $\boldsymbol{I} \in \mathbb{R}^{7\times7}$ is the identity matrix. The last row ensures that a comfortable realistic pose is created. The matrix $\boldsymbol{P}$ performs a projection onto the nullspace of $\boldsymbol{J}_{pos}$ and $\boldsymbol{J}_{or}$ (see [10]). A movement of the joints in this nullspace has no effect on the position and orientation of the end-effector. Thus, such a movement is suitable to pursue the secondary target of reaching a comfortable realistic pose. The vector $\boldsymbol{q}_{guess} \in \mathbb{R}^7$ points in joint angle space in the direction of a natural looking guess posture, which does not necessarily needs to reach $\boldsymbol{r}^i_{ref}$ and $\boldsymbol{T}^i_{ref}$ exactly. The vector $\boldsymbol{q}_{guess}$ is projected in the nullspace to create a movement as close as possible in the direction of $\boldsymbol{q}_{guess}$ without changing the position and orientation. The calculation of $\boldsymbol{q}_{guess}$ is different for the upper and lower limbs.

For the upper limbs the sensorimotor transformation model (STM) from [26] is used for setting the superfluous DOF. Such experimentally derived models are a robust way to generate realistic postures and were also used in other works like [17] or [28]. The STM linearly describes the relation between the wrist position and the arm pose a human would take. The difference between the current joint angles and the angles coming from the STM is used as $\boldsymbol{q}_{guess}$. For the lower limbs $\boldsymbol{q}_{guess}$ points in the direction of a predefined comfortable posture for the ankle joints. As a comfortable ankle posture a minimal axial rotation of the knee is assumed.

For the upper limbs of the DHM an additional algorithm ensures the collision avoidance between the torso and the lower arm as well as the torso and the elbow. For this purpose, the torso is approximated as a prism. During the iteration process the joint limits $\boldsymbol{q}^i_{min}$ and $\boldsymbol{q}^i_{max}$ for $i \in [1, 2]$ are adapted dynamically so that a collision with the approximated torso geometry is not possible without violating the joint limits.

Fig. 1 shows that natural looking poses are derived with the proposed approach. Summarized, the introduced IK algorithm calculates the joint angles $\boldsymbol{q}^i_{ref}$ resulting in $\boldsymbol{r}^i_{ref}$ and $\boldsymbol{T}^i_{ref}$ being reached within the range of motion of the human. The superfluous DOF is used to approximate the joint angles to an natural looking posture calculated with the STM for the upper limbs, or to the comfortable ankle posture for the lower limbs. For the upper limbs collision avoidance with the torso is ensured.

C. Human Inspired Control Scheme for the Limbs

After calculating the reference joint angles $\boldsymbol{q}^i_{ref}$ as described in the previous section, each limb's joints can be controlled to execute the desired movement. In order to produce meaningful results in situations like aircraft-pilot coupling, mentioned in section I, the behavior of the proposed controller takes the most important aspects of human motor control into account. In this paper, it is not the scope of the controller to model exact human behavior. It is merely used to approximate the human motor control. Fig. 3 shows the control scheme for the limbs in the context of the whole DHM.

It is assumed in literature that the central nervous system (CNS) adapts muscle forces in a predictive manner to compensate for interaction torques arising at one joint due to the motion of limb segments around another joint [13]. For this reason a feed forward inverse dynamics model of the limb is part of the scheme. The inverse dynamics model

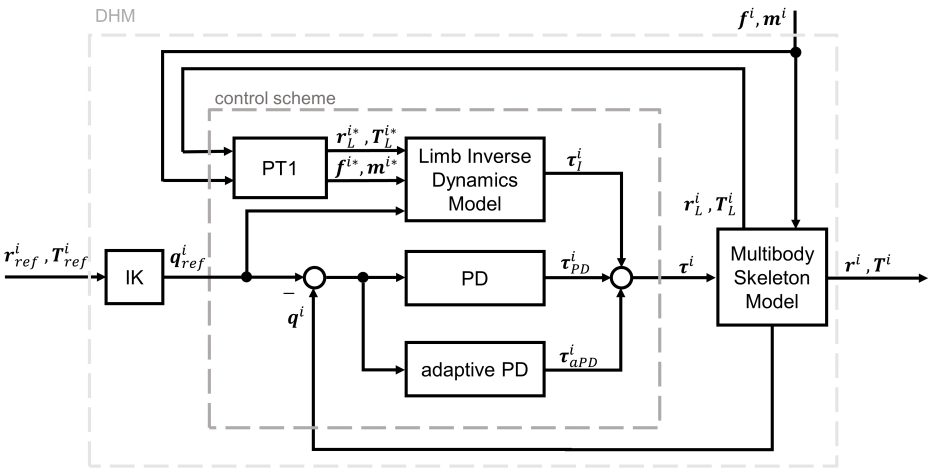

Fig. 3. Proposed control scheme for the limbs in context of the entire DHM. The used control scheme with an inverse dynamics model, an adaptive PD-controller and simplified consideration of reaction time is inspired by the control behavior of the central nervous system.

has the filtered values of the position $\boldsymbol{r}_L^i$ and orientation $\boldsymbol{T}_L^i$ as inputs. For the lower limbs they describe the position and orientation of the hip joint, for the upper limbs of the shoulder. Also the filtered forces $\boldsymbol{f}^i$ and torques $\boldsymbol{m}^i$ acting on the end-effector due to interaction with the environment are inputs. The last input is $\boldsymbol{q}_{ref}^i$. The inverse dynamics model determines the needed torques $\boldsymbol{\tau}_I^i$ for the limbs joints to follow $\boldsymbol{q}_{ref}^i$.

The inputs $\boldsymbol{f}^{i*}$, $\boldsymbol{m}^{i*}$, $\boldsymbol{r}_L^{i*}$ and $\boldsymbol{T}_L^{i*}$ of the inverse dynamics model are the PT1-filtered values $\boldsymbol{f}^i$, $\boldsymbol{m}^i$, $\boldsymbol{r}_L^i$ and $\boldsymbol{T}_L^i$. For $\boldsymbol{T}_L^i$ it is made sure that a valid orientation matrix results by normalizing the corresponding quaternion. The filtering is done to prevent a immediate reaction of the control scheme to external influences and to introduce an approximation of a human reaction time. Without using any reaction time model the controller would adapt $\boldsymbol{\tau}_I^i$ instantly to a change of external influences like vehicle accelerations, resulting in no joint deflections. An observation of dynamic interaction with the environment would then be impossible. Assuming the response of the CNS with a PT1 behavior is a strong simplification which leaves space for further work. The input $\boldsymbol{q}_{ref}^i$ is not filtered, because it describes the intended movement to which there is no need to react.

The PD-controller in Fig. 3 corrects the torques $\boldsymbol{\tau}_I^i$ by $\boldsymbol{\tau}_{PD}^i$ with

$$\boldsymbol{\tau}_{PD}^i = \boldsymbol{K}^i \cdot \boldsymbol{\varepsilon}^i + \boldsymbol{D}^i \cdot \dot{\boldsymbol{\varepsilon}}^i \tag{6a}$$

$$\boldsymbol{\varepsilon}^i = \boldsymbol{q}_{ref}^i - \boldsymbol{q}^i \tag{6b}$$

where $\boldsymbol{K}^i \in \mathbb{R}^{7\times7}$ is the diagonal stiffness matrix and $\boldsymbol{D}^i \in \mathbb{R}^{7\times7}$ is the diagonal damping matrix. The PD-controller is used to model the impedance of the arm due to friction and stiffness of the muscles. The PD-controller creates a stationary accurate behavior of the whole control scheme. $\boldsymbol{K}$ and $\boldsymbol{D}$ are optimized for a good controller guidance behavior of the limbs without consideration of interaction of the end-effector with the environment.

In interaction with the environment, the behavior of the PD-controller can thus get unstable. To prevent this, a human-like adaption of stiffness and damping of the joints like proposed in [29] is used and described below. It models the adaption of muscle tension by the human in unstable interaction situations. The tracking error $\boldsymbol{\varepsilon}_{track}^i \in \mathbb{R}^7$ is defined by

$$\boldsymbol{\varepsilon}_{track}^i = \boldsymbol{\varepsilon}^i + \kappa \cdot \dot{\boldsymbol{\varepsilon}}^i \tag{7a}$$

The constant κ sets the proportion for $\boldsymbol{\varepsilon}_{track}^i$ between the position error $\boldsymbol{\varepsilon}^i \in \mathbb{R}^7$ and velocity error $\dot{\boldsymbol{\varepsilon}}^i \in \mathbb{R}^7$. The torques $\boldsymbol{\tau}_{aPD}^i$ coming from the adaptive PD-controller are calculated with

$$\boldsymbol{\tau}_{aPD}^i = \boldsymbol{K}_a^i \cdot \boldsymbol{\varepsilon}^i + \boldsymbol{D}_a^i \cdot \dot{\boldsymbol{\varepsilon}}^i. \tag{8}$$

$\boldsymbol{K}_a^i \in \mathbb{R}^{7\times7}$ is the adaptive stiffness matrix and $\boldsymbol{D}_a^i \in \mathbb{R}^{7\times7}$ is the adaptive damping matrix. Their derivatives are calculated with

$$\dot{\boldsymbol{K}}_a^i = \boldsymbol{Q}_P^i \cdot (\boldsymbol{\varepsilon}_{track}^i \cdot \boldsymbol{\varepsilon}^{i^T} - \gamma^i \cdot \boldsymbol{K}_a^i) \tag{9}$$

$$\dot{\boldsymbol{D}}_a^i = \boldsymbol{Q}_D^i \cdot (\boldsymbol{\varepsilon}_{track}^i \cdot \dot{\boldsymbol{\varepsilon}}^{i^T} - \gamma^i \cdot \boldsymbol{D}_a^i) \tag{10}$$

$$\gamma^i = \frac{a}{1 + b \cdot ||\boldsymbol{\varepsilon}_{track}^i||}. \tag{11}$$

The start entries of $\boldsymbol{K}_a^i$ and $\boldsymbol{D}_a^i$ are set to zero at the beginning of the simulation. The entries of $\boldsymbol{K}_a^i$ and $\boldsymbol{D}_a^i$ adapt over time depending on $\boldsymbol{\varepsilon}_{track}^i$, $\boldsymbol{\varepsilon}^{i^T}$ respectively $\dot{\boldsymbol{\varepsilon}}^{i^T}$ and the forgetting rate γ^i in order to prevent unstable behavior. With the weighting matrices $\boldsymbol{Q}_P^i \in \mathbb{R}^{7\times7}$ and $\boldsymbol{Q}_D^i \in \mathbb{R}^{7\times7}$ the learning or forgetting for each joint can be scaled. For the DHM $\boldsymbol{Q}_P^i$ and $\boldsymbol{Q}_D^i$ are diagonal matrices. The entries of the matrices are selected in the same proportion to each other as the constants of the PD-controller. This results e.g. in a higher scaling of the learning for a shoulder joint than for a wrist joint.

Equation (11) describes the forgetting rate γ^i. It depends on the current tracking error $\boldsymbol{\varepsilon}_{track}$ as well as on the two constants a and b. The higher γ^i the faster the learned stiffness and damping decomposes, which can be seen in (9) and (10).

The joint torques $\boldsymbol{\tau}^i = \boldsymbol{\tau}_I^i + \boldsymbol{\tau}_{PD}^i + \boldsymbol{\tau}_{aPD}^i$ are limited to maximum values so that $\boldsymbol{\tau}^i \in [\boldsymbol{\tau}_{min}^i; \boldsymbol{\tau}_{max}^i]$ holds true. The limits for $\boldsymbol{\tau}^i$ are based on literature values for average men and women [14], [12], [22], [18], [15], [21].

With the inverse dynamics model, the PD-controller and the adaptive PD-controller the introduced controller for the DHM ensures a stable control of the limbs inspired by human motor control.

III. Pilot-aircraft Coupling Analysis during Gust as Use Case for the Human Model

As use-case to demonstrate the capabilities of the human model a pilot in the loop simulation for a sports aircraft encountering a gust is performed. The dynamic behavior of the aircraft is analyzed afterwards with respect to aircraft-pilot coupling.

A. Aircraft Model

The "Airplane A" [24, Chapter 11], which is similar to a Cessna 172 [1], is used. The aircraft is modeled as a 6-DOF point mass of mass m and with an inertia matrix $\boldsymbol{I}$ on a flat earth. Let ${}^{O}\boldsymbol{r} \in \mathbb{R}^3$ denote the aircraft's position in the north-east-down coordinate system $\mathcal{F}_O$. Furthermore, let ${}^{O}\boldsymbol{\Theta} = \begin{bmatrix}\phi & \theta & \psi\end{bmatrix} \in \mathbb{R}^3$ denote the Euler angles to rotate the north-east-down system into the body system $\mathcal{F}_B$, which is fixed to the aircraft's reference point and pointing towards the nose, starboard, and downwards. Additionally, ${}^{B}\boldsymbol{v} \in \mathbb{R}^3$ is the flight velocity in $\mathcal{F}_B$ and ${}^{B}\boldsymbol{\omega} \in \mathbb{R}^3$ are the angular rates in $\mathcal{F}_B$. The motion of the point mass in space is influenced solely by the acting forces $\boldsymbol{f}$ and moments $\boldsymbol{m}$ and is described by the Euler-Newton equations of motion

$$m\left({}^{B}\dot{\boldsymbol{v}} + {}^{B}\boldsymbol{\omega} \times {}^{B}\boldsymbol{v}\right) = {}^{B}\boldsymbol{f}_{\text{aero}} + {}^{B}\boldsymbol{f}_{\text{prop}} + {}^{B}\boldsymbol{f}_{\text{g}} \tag{12}$$

$$\boldsymbol{I}\,{}^{B}\dot{\boldsymbol{\omega}} + {}^{B}\boldsymbol{\omega} \times \boldsymbol{I}\,{}^{B}\boldsymbol{\omega} = {}^{B}\boldsymbol{m}_{\text{aero}} + {}^{B}\boldsymbol{m}_{\text{prop}} \tag{13}$$

where the indices $_{\text{aero}}$ denotes aerodynamic forces and moments, $_{\text{prop}}$ propulsion-induced effects, and $\boldsymbol{f}_{\text{g}}$ the gravitational force. Propulsion forces ${}^{B}\boldsymbol{f}_{\text{prop}}$ and moments ${}^{B}\boldsymbol{m}_{\text{prop}}$ are assumed to act in forward direction only. Furthermore, the torque τ_{prop} is assumed to depend on the thrust $T_{\text{prop}} \in [0\ \text{N}; 2700\ \text{N}]$ linearly through the coefficient $C_{\text{q}} = 0.1$ m, i.e., $\tau_{\text{prop}} = C_{\text{q}}\ T_{\text{prop}}$. The aerodynamic forces ${}^{B}\boldsymbol{f}_{\text{aero}}$ and moments ${}^{B}\boldsymbol{m}_{\text{aero}}$ are calculated by using the coefficients from [24, Table 11.1].

As for the DHM, the `Modelica` language is used to implement the aircraft model. Figure 4 shows the implemented aircraft model.

B. Coupled Aircraft-Pilot Model

The simulation model for the use-case consists of the aircraft model from section III-A, the proposed DHM used as pilot, a simplified model of the flight stick and the cable pulls of the aircraft as well as a PID-controller together with the stick and cable pulls kinematics.

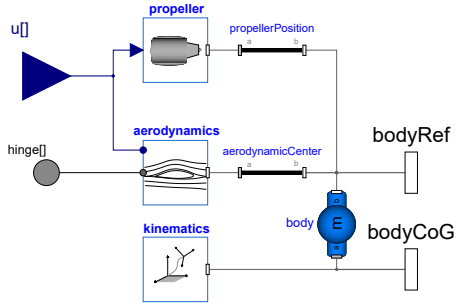

Fig. 4. Modelica block diagram of the implemented aircraft.

Fig. 5 illustrates the interaction of the submodels mentioned above. The dashed box shows the coupling of the human body with the aircraft. The pose $(\boldsymbol{r}^1, \boldsymbol{T}^1)$ of the right hand holding the stick is controlled to the reference pose $(\boldsymbol{r}^1_{ref}, \boldsymbol{T}^1_{ref})$ by the pilot model (see Fig. 3). The forces $\boldsymbol{f}^1$ and torques $\boldsymbol{m}^1$ acting between the hand and the stick as well as the aircraft accelerations ${}^{B}\dot{\boldsymbol{v}}$ and ${}^{B}\dot{\boldsymbol{\omega}}$ act as disturbances on the DHM. The buttocks of the DHM are connected rigidly to the aircraft. The left hand and the feet are not connected to the aircraft.

The pose of the right hand is transformed to the flaps angles φ_{ail} and φ_{ele} due to the transmission of the stick and the cable pulls. The stick has two rotational DOF. The first one is the angle to the side φ^*_{ail} to move the ailerons. The second is the angle to the front φ^*_{ele} to move the elevator. The cable pulls are modeled simplified as a fixed gearing ratio n_G between the sticks and flaps angles. The friction and flexibility in the cable pulls is neglected for this use-case. The relations between the flaps and the sticks quantities marked with * are described by

$$\varphi^*_{ail} = \varphi_{ail} \cdot n_G \tag{14a}$$

$$\varphi^*_{ele} = \varphi_{ele} \cdot n_G \tag{14b}$$

$$\tau_{ail} = \tau^*_{ail} \cdot n_G \tag{14c}$$

$$\tau_{ele} = \tau^*_{ele} \cdot n_G \tag{14d}$$

The torques τ_{ail} and τ_{ele} acting on the flaps are calculated by the aircraft aerodynamics. These lead to $\boldsymbol{f}^1$ and $\boldsymbol{m}^1$ acting on the hand due to the sticks lever arm.

The roll angle ϕ of the aircraft-pilot system is controlled with a PID controller calculating $\varphi_{ail,ref}$ (see Fig. 5). It represents simplified the cognitive level of the pilot adjusting the reference angle $\varphi_{ail,ref}$ he wants to set by means of the stick. The used PID controller is slow compared to the controller of the limbs from section II-C ensuring that the two controllers do not interfere with each other. With the sticks and cable pulls kinematics the required hand pose $(\boldsymbol{r}^1_{ref}, \boldsymbol{T}^1_{ref})$ results from $\varphi_{ail,ref}$. For the pitch angle θ no controller is required because the aircraft model shows a stable behavior around the pitch axis. Therefore the elevator reference angle is fixed to $\varphi_{ele,ref} = 0$.

The chosen cockpit layout defining the positions of stick, seat and the feet is based on the civil cockpit layout for center stick controlled airplanes from [23]. The resulting posture of the DHM can be seen in Fig. 1. For the pilot a body weight of 80 kg and the proportions of a 50^{th} percentile male according to [3] are chosen.

During the simulation of a straight flight in 1500 m altitude a 1-cosine gust is acting on the aircraft. The gust velocity is described by

$$v_{gust} = \begin{cases} 0\ \text{m/s} & \text{for } t < t_0 \\ 0\ \text{m/s} & \text{for } t_0 + \Delta t < t\ . \\ A \cdot (1 - \cos(2\pi \cdot \frac{t - t_0}{\Delta t})) & \text{else} \end{cases} \tag{15}$$

With $t_0 = 0.5$ s, $\Delta t = 0.5$ s and $A = 28$ m/s. The direction of the gust is described by the vector $r_{gust} = [0, 1, 1]$. It is a strong and short gust resulting in high hinge moments τ_{ail}

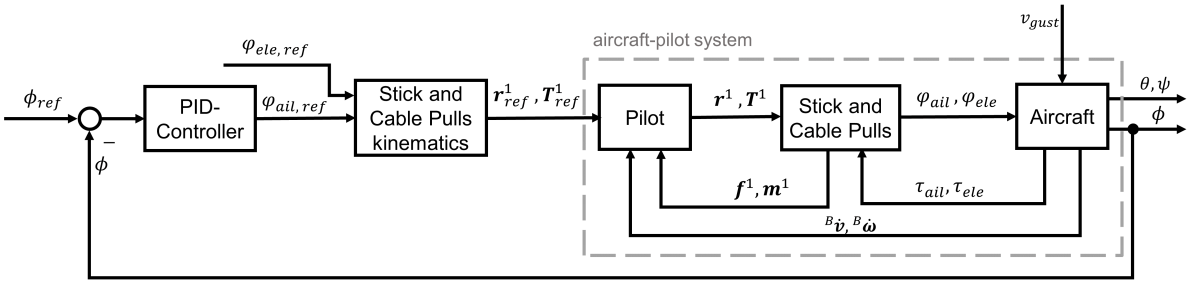

Fig. 5. Block diagram of the pilot in the loop. The DHM actuates the flight stick in order to adjust the flaps to the reference angels $\varphi_{ail,ref}$ and $\varphi_{ele,ref}$. The slow PID-controller represents the cognitive level of the pilots behavior by adjusting the reference angle $\varphi_{ail,ref}$ to reach ϕ_{ref} by means of the DHM. For the pitch angle θ no controller is required because the pilot aircraft model shows a stable behavior around the pitch axis. The reference angle for the elevator is $\varphi_{ele,ref} = 0$.

and τ_{ele} and aircraft accelerations ${}^B\dot{\boldsymbol{v}}$ and ${}^B\dot{\boldsymbol{\omega}}$. It allows a better observation of the dynamical effects predicted by the human model than on a longer mild gust.

The dynamic behavior of the described aircraft-pilot system during the influence of the gust is simulated for two different time constants $T_r = 0.1$ s and $T_r = 0.2$ s of the PT1-filter from Fig. 3 to compare the effect of different reaction times on the simulation results. For these two conditions the pilot has the full strength (FS) of a average male with respect to the joints torque limits. A third condition with a reduced strength (RS) of the pilot by 20% is simulated where one joint of the arm reaches its maximum torque.

IV. Simulation Results

This section outlines the simulation results of the three considered conditions. It turns out that the dynamical behavior of the pilot influences the aircraft behavior in the simulation. It further can be seen that the DHM shows a plausible conduct during the interaction with the aircraft model.

Attention is drawn to the fact that the considered aircraft model is a simplified model. This is especially the case for the flight stick with the cable pulls. It is not claimed that the model is an adequate representation of a real aircraft's behavior. Also the proposed control scheme for the limbs, in particular the modeling of the reaction time, is a strong simplification of the reality. Nevertheless, the use-case is suitable to investigate the capabilities of the DHM to simulate the key aspects of human body dynamics in a highly dynamic environment.

Fig. 6 shows the sidewards deflection of the stick φ^*_{ail} during the simulated flight in the first plot. In the second plot the forward/ backward deflection φ^*_{ele} is shown. Both plots have a characteristic course over time for all three conditions. During the gust the biggest deflections away from the reference stick angles occur. It can be explained by a combination of torques acting on the stick and accelerations of the aircraft both resulting from the aircrafts aerodynamics. With the gust velocity decreasing from $t = 0.75$ s the hinge moments and aircraft accelerations are decreasing, too. Due to the consideration of reaction time in the control scheme the arm's joint torques $\boldsymbol{\tau}^i$ decrease with a phase shift. This leads to the observed overshoot for both stick angles between $t = 1$ s and $t = 1.5$ s. For the first condition additionally

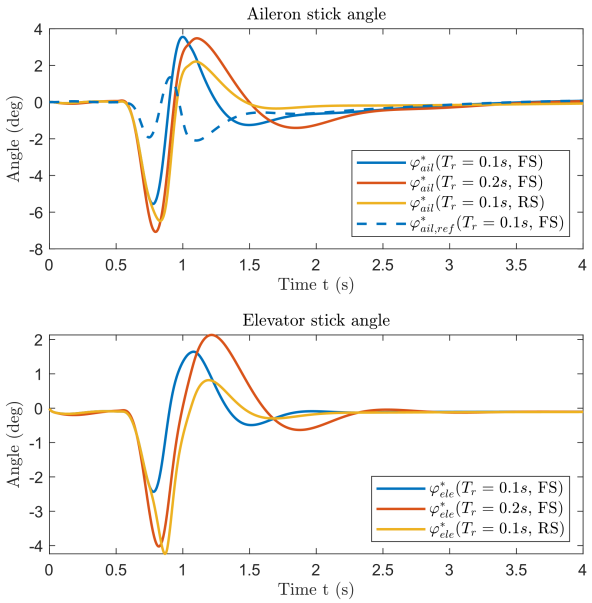

Fig. 6. Angles of the flight stick during the influence of the gust for the three simulated conditions. The dotted line additionally shows the reference Angle $\varphi^*_{ail,ref}$ for the first condition. The gust is starting at $t = 0.5s$ with a duration of $t = 0.5s$.

the stick's reference angle $\varphi^*_{ail,ref}$ is plotted. The figure shows nicely that the influence of the simulated human body dynamics on the aircraft-pilot system is significant between $t \approx 0.5$ s and $t \approx 2$ s. In this time slot the hand is not able to follow the reference stick angles precisely due to the dynamic influences of the aircraft. It is also visible that the phase shift between the peaks of $\varphi^*_{ail,ref}$ and φ^*_{ail} increases over time. A longer lasting turbulence thus could lead to unstable behavior of the simulated aircraft-pilot system. After $t \approx 2$ s the stick follows $\varphi_{ail,ref}$ in a small tolerance again.

The observed differences between the three conditions in Fig. 6 show that the parameterisation of T_r has a significant impact on the stick's angles and thus also on the aircraft-pilot system. With a higher reaction time the deflection of the stick during the gust is also higher. It is pointed out that no PT1-filtering before the inverse dynamics model would mean $T_r = 0$ s. This would result in no stick deflection off the reference angles due to a immediate adaption of the joint torques. Therefore, the role of considering the reaction time

is essential for representing dynamic human behavior. And also the validity of the used reaction time model has great significance on the validity of the whole DHM due to it's effects on the simulation results (see Fig. 6). Implementing a more realistic model of human reaction in motor control thus is a important step to get reliable results with the DHM. For the comparison of the first (blue line) and the third condition (yellow line) it can bee seen that both lines are equal until $t \approx 0.7$ s. This is the time where one shoulder joint reaches its maximum torque.

Fig. 7 shows the utilization rate of the third DOF of the shoulder joint. It is the most charged joint of the arm mainly contributing to the sidewards stick movement. For the third condition a utilization rate of 100% is reached due to reduced maximum joint torques by 20%. At the maximum utilization rate this joint's torques can't be increased by the controller any more. In consequence, the stick deflection increases from $t \approx 0.7$ s in Fig. 6 in comparison to the first condition.

Fig. 8 shows the two most important variables, namely torque and joint deflections, for all seven swivel joints of the right arm for the RS condition. The first plot shows the deflections off the reference joint angles $\boldsymbol{q}_{err} = \boldsymbol{q}^1_{ref} - \boldsymbol{q}^1$. During the gust every joint is deflected due to the forces acting on the hand and the accelerations acting on the aircraft. The third swivel joint has the biggest deflection resulting from reaching the maximum torque for this joint. In the second plot the joint torques are shown. Due to the adaption of the joint torques by the controller, mainly visible between $t \approx 0,5$ s and $t \approx 1,5$ s, the deflections go back to nearly zero again after the gust. For the third joint it can be seen that the maximum torque is reached between $t \approx 0,7$ s and $t \approx 0,9$ s.

Fig. 9 shows the roll angle ϕ and yaw angle ψ during and after the gust. The pitch angle θ is not shown because nearly no differences for the three simulated conditions occurred. This may be due to the stable behavior of the aircraft model around the pitch axis mentioned above. In Fig. 9 the impact of the stick deflections on the aircraft becomes visible. Both angles only move within a tight range. Nevertheless, a different aircraft behavior can be observed for the three conditions due to the human factor.

For better understanding of Fig. 9 it has to be mentioned that $\phi \neq 0$ results in a yaw rate $\dot{\psi} \neq 0$ due to the aircrafts

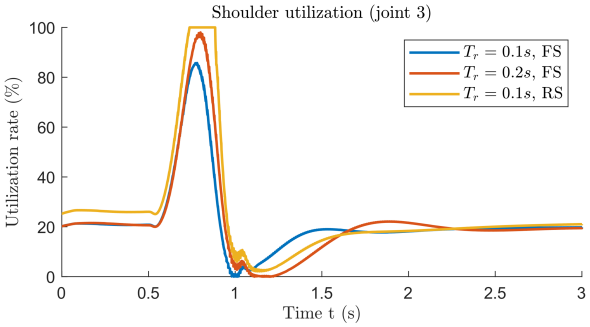

Fig. 7. Utilization rate of the third shoulder DOF which describes the rotation around the upper arms axis. In the third condition the maximum joint torques are decreased by 20%. In consequence this joint reaches 100% of its maximum torque during the gust.

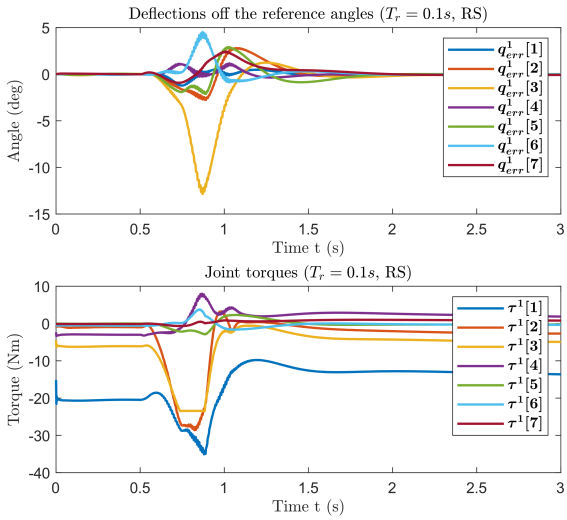

Fig. 8. Deflections of the right arms swivel joints off the reference joint angles $\boldsymbol{q}^i_{ref}$ (first plot). During the gust every swivel joint is deflected. The biggest deflection occurs for the third swivel joint, that reaches its torque limit. In order to compensate for the deflections the controller adapts the joint torques shown in the second plot.

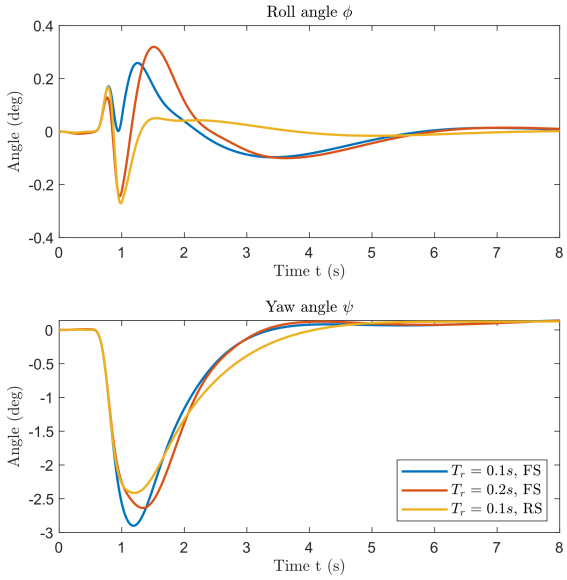

Fig. 9. Roll angle ϕ and yaw angle ψ of the aircraft during the simulation. The influence of the human body on the aircraft-pilot dynamics becomes clear by the different resulting courses for the three conditions.

aerodynamics. The yaw angle is also highly influenced by the side wards proportion of the gust generating a force on the rudder and thus causing the aircraft to accelerate around the vertical axis.

The first peak of ϕ and the decrease of ψ look similar between $t = 0.5$ s and $t \approx 0.8$ s for all three conditions. In this time slot the movement of the aircraft is dominated by the accelerations caused by the gust. For $t \geq 0.8$ s the three lines start to diverge. Here the effects of the differently deflected stick for each condition due to the human factor start to matter. The following oscillations of ϕ are a consequence of the stick oscillations from Fig. 6. The above mentioned correlation of ϕ and ψ is responsible for

the diverging courses of ψ. It is interesting to note that in this particular example the last two conditions lead to a smaller peak of ψ. That suggests that the unintended stick deflections have a damping effect around the down axis on the simplified aircraft model during the gust. It is also worth mentioning that the roll angle ϕ goes back to nearly zero very fast for the third condition compared to the first two conditions. Easing the grip at the stick during the gust combined with the lower reaction time has thus the most stabilizing effect on the roll movement of the three considered conditions because of the inherent stable behavior of the aircraft dynamics.

Summarized it can be said that an impact of the human body dynamics on the pilot aircraft system is shown by the results of the use-case simulation. Furthermore the general behavior of the DHM as well as the differences in the dynamic behavior of the aircraft-pilot system that occurred for different parameterisations of the DHM are plausible.

V. Conclusion

In this study a DHM for the purpose of dynamic analysis is presented. It is the first model of this kind implemented in the modeling language `Modelica`. The implementation in `Modelica` allows a use of the DHM across domains. The model consists of three main parts. The multi-body skeleton model, an IK-algorithm for the limbs and the control scheme inspired by human motor control.

The use-case simulation considered in this paper shows a significant impact of the human body dynamics on the aircraft-pilot system under the influence of a 1-cosine gust. It is also shown that a different parameterisation of the DHM concerning the pilots reaction time and strength is leading to a plausible different behavior of the aircraft-pilot system. This suggests that the used approach to model the human body is capable of taking the substantial dynamic effects of the human body in dynamic human-machine interactions into account.

For a meaningful use of the model further work is required. One is the improvement of the proposed controller for the limbs and a comparison of its behavior with real human conduct in motor control. Especially the replacement of the PT1-filter of the controller with a more sophisticated model of human reaction to external influences is an important step. Testing the model in a more realistic use-case e.g. without neglecting the influences of friction and flexibility in the cable pulls would make it possible to compare the results to known aircraft-pilot behavior. Last a validation of the DHM's predictions is important to evaluate significance and limits of the model.

References

[1] *Pilot's Operating Handbook Cessna C172*. The Cessna Aircraft Company, 1998.

[2] *Anthropometry*, chapter 4, pages 82–106. John Wiley & Sons, Ltd, 2009.

[3] Din 33402 -2 Ergonomie –Körpermaße des menschen –Teil 2: Werte. *Deutsches Institut für Normung*, 2020.

[4] *RAMSIS Software*. https://www.human-solutions.com/en/products/ramsis-general/start.html, last accessed: 11.03.2022.

[5] *AnyBody Software*. https://www.anybodytech.com/software/, last accessed: 24.6.21.

[6] *Siemens PLM Software*. https://www.plm.automation.siemens.com/global/en/products/manufacturing-planning/human-centered-design-simulation.html, last accessed: 24.6.21.

[7] *OpenSim Software*. https://opensim.stanford.edu/work/index.html, last accessed: 29.6.21.

[8] Hess Ronald A. Theory for aircraft handling qualities based upon a structural pilotmodel. *Journal of Guidance, Control, and Dynamics*, 12(6):792–797, 1989.

[9] Jan Boril, Rudolf Jalovecky, and Rashid Ali. Human - Machine Interaction and Simulation Models Used in Aviation. 2013.

[10] Samuel R. Buss. Introduction to Inverse Kinematics with Jacobian Transpose, Pseudoinverse and Dampedleast Squares methods. 2004.

[11] Florian Engstler and Heiner Bubb. Generation of Percentile Values for Human Joint Torque Characteristics. *Conference: Digital Human Modeling, Second International Conference*, 2009.

[12] Fabian Günzkofer, H. Bubb, and Klaus Bengler. Elbow Torque Ellipses: Investigation of the mutual influences of rotation, flexion, and extension torques. *Work: A Journal of Prevention, Assessment and Rehabilitation*, 41(Supplement 1/ 2012):2260–2267, 2012.

[13] Paul L. Gribble and David J. Ostry. Compensation for Interaction Torques During Single- and Multijoint Limb Movement. *Journal of Neurophysiology*, 82(5):2310–2326, nov 1999.

[14] Fabian Guenzkofer, Florian Engstler, Heiner Bubb, and Klaus Bengler. Isometric elbow flexion and extension joint torque measurements considering biomechanical aspects. 01 2011.

[15] Thomas Harbo, John Brincks, and Henning Andersen. Maximal isokinetic and isometric muscle strength of major muscle groups related to age, body mass, height, and sex in 178 healthy subjects. *European journal of applied physiology*, 112:267–75, 05 2011.

[16] Saul Katherine, Murrayand Wendy, and Delp Scott. A Model of the Upper Extremity for Simulating Musculoskeletal Surgery and Analyzing Neuromuscular Control. *Annals of biomedical engineering*, 33:829–40, 07 2005.

[17] Koichi Kondo. Inverse Kinematics of a Human Arm. *Robotics Laboratory Department of Computer Science, Stanford University*, 1996.

[18] A.V. Koski and S.M. McGill. Dynamic shoulder flexion strength: for use in occupational risk analysis and clinical assessment. *Clinical Biomechanics*, 9(2):99–104, 1994.

[19] Sebastian Kümper, Matthias Hellerer, and Tobias Bellmann. DLR Visualization 2 Library - Real-Time Graphical Environments for Virtual Commissioning. In Martin Sjölund, Lena Buffoni, Adrian Pop, and Lennart Ochel, editors, *14th Modelica Conference*, pages 197–204. Modelica Association and Linköping University Electronic Press, September 2021.

[20] Duane T. McRuer and E. Krendel. Mathematical models of human pilot behavior. *AGARDograph No.188*, 1974.

[21] Katherine Plewa, Jim R. Potvin, and James P. Dickey. Wrist rotations about one or two axes affect maximum wrist strength. *Applied Ergonomics*, 53:152–160, 2016.

[22] D.C. Reid, G. Oedekoven, J.F. Kramer, and L.A. Saboe. Isokinetic muscle strength parameters for shoulder movements. *Clinical Biomechanics*, 4(2):97–104, 1989.

[23] Jan Roskam. *Ariplane Design Part III: Layout Design of Cockpit, Fuselage, Wing and Empenage: Cutaways and Inboard Profiles*. Roskam Aviation and Engineering Corporation, 1986.

[24] Jan Roskam. *Airplane Design Part VI: Preliminary calculations of aerodynamic thrust and power characteristics*. Roskam Aviation and Engineering Corporation, 1987.

[25] Günter Schreiber, Martin Otter, and Gerd Hirzinger. Solving the Singularity Problem of non-redundant Manipulators by Constraint Optimization. *German Aerospace Center - DLR Institute for Robotics and System Dynamics*, 1999.

[26] John F. Soeching and Martha Flanders. Errors in Pointing are Due to Approximations in Sensorimotor Transformations. *Journal of Neurophysiology*, 1989.

[27] Qihan Wang, Gang Zhou, Zhenming Liu, and Bin Ren. Building a skeleton-based 3d body model with angle sensor data. *Smart Health*, 2021.

[28] Yuting Wang and Panagiotis Artemiadis. Closed-Form Inverse Kinematic Solution for Anthropomorphic Motion in Redundant Robot Arms. *Advances in Robotics & Automation*, 2013.

[29] Chenguang Yang, Gowrishankar Ganesh, Sami Haddadin, Sven Parusel, Alin Albu-Schäeffer, and Etienne Burdet. Human-Like Adaptation of Force and Impedance in Stable and Unstable Interactions. *IEEE TRANSACTIONS ON ROBOTICS*, 2011.

[30] Andrea Zanoni, Alessandro Cocco, and Pierangelo Masarati. Multibody dynamics analysis of the human upper body for rotorcraft–pilot interaction. *Nonlinear Dynamics*, 2020.